Brain Imaging and Behavior
DOI 10.1007/s11682-017-9697-8

ORIGINAL RESEARCH

# Brain functional connectivity in lung cancer population: an exploratory study

M. Simó[1,2] · X. Rifà-Ros[1,3] · L. Vaquero[1] · P. Ripollés[1,3] · N. Cayuela[2] · J. Jové[4] · A. Navarro[5] · F. Cardenal[6] · J. Bruna[2] · Antoni Rodríguez-Fornells[1,3,7]



**Abstract** The present study aimed to explore the functional connectivity differences in Resting State Networks (RSNs) induced by cancer and chemotherapy in Lung Cancer (LC) patients using an Independent Component Analysis (ICA). Three matched groups of 15 LC patients following Chemotherapy (C+), 15 LC patients before Chemotherapy (C-) and 15 Healthy Controls (HC) were included. Analysis was performed using ICA and a multivariate pattern analysis (MVPA) to classify groups based on profiles of functional connectivity. We found significant differences in four of the RSN identified: Default Mode Network (DMN), Predominantly Left and Right Anterior Temporal Network, and Cerebellum Network. Whereas DMN showed decreased connectivity, the other RSNs exhibited increased connectivity in both LC groups compared to HC and in C+ in comparison to C-. MVPA discriminated significantly and accurately between all groups. Our study showed that disrupted functional connectivity associated with cancer and chemotherapy-induced cognitive deficits is not only related to DMN decreased connectivity abnormalities but also to an increased connectivity of other RSNs, suggesting a potential compensatory mechanism.

**Keywords** Resting-state functional magnetic resonance imaging · Chemotherapy · Lung cancer · Default mode network · Functional connectivity

## Introduction

Chemotherapy-induced cognitive impairment or 'chemobrain' is a well-recognized clinical syndrome, consisting of subtle to mod-

M. Simó and X. Rifà-Ros contributed equally to this work

J. Bruna and A. Rodríguez-Fornells share co-senior authorship

**Electronic supplementary material** The online version of this article (doi:10.1007/s11682-017-9697-8) contains supplementary material, which is available to authorized users.

✉ Antoni Rodríguez-Fornells
antoni.rodriguez@icrea.cat

[1] Cognition and Brain Plasticity Group, Bellvitge Biomedical Research Institute-IDIBELL, L'Hospitalet de Llobregat, 08907 Barcelona, Spain

[2] Neuro-Oncology Unit, Hospital Universitari de Bellvitge-ICO L'Hospitalet-IDIBELL, 08907 Barcelona, Spain

[3] Department of Basic Psychology, Campus Bellvitge, University of Barcelona, L'Hospitalet de Llobregat, 08907 Barcelona, Spain

[4] Radiation Oncology Department, Hospital Germans Trias i Pujol, ICO Badalona, 08916 Barcelona, Spain

[5] Lung Cancer Unit, Radiation Oncology Department, ICO L'Hospitalet, 08907 Barcelona, Spain

[6] Lung Cancer Unit, Medical Oncology Department, ICO L'Hospitalet, 08907 Barcelona, Spain

[7] Catalan Institution for Research and Advanced Studies, ICREA, 08010 Barcelona, Spain

Published online: 13 March 2017

erate cognitive changes across various domains (Jim et al. 2012). Although acute cognitive changes during chemotherapy are common (Ahles et al. 2002), long-term cognitive changes post-treatment seem to persist only in a subgroup (17–34%) of cancer survivors (Ahles and Saykin 2007). In addition, cognitive deficits have also been described in cancer patients prior to chemotherapy (Ahles and Saykin 2002). In recent years, several studies using neuroimaging techniques, concretely magnetic resonance imaging (MRI) and positron emission tomography, have reported structural and functional connectivity brain changes associated with cancer and chemotherapy (Kesler 2014; Simo et al. 2013).

Resting-state functional magnetic resonance imaging (RS-fMRI) is a non-invasive method for examining the intrinsic topology of synchronous large-scale brain networks, occurring when a subject is not performing an explicit task (Lee et al. 2013; Wang et al. 2010). Thus, RS-fMRI is well-suited to assess the intrinsic connections that are believed to support cognitive functioning (Church et al. 2009) and has been repeatedly used to understand the nature of functional connectivity across both healthy subjects and several clinical populations (i.e., Alzheimer disease (Sanz-Arigita et al. 2010), schizophrenia (Lynall et al. 2010). However, to date only a handful of studies have used RS-fMRI to study the neurobiological mechanisms underlying the cognitive impairment associated with cancer and chemotherapy (Bruno et al. 2012; Dumas et al. 2013; Kesler 2014; Piccirillo et al. 2015).

Early studies, (Dumas et al. 2013; LaViolette et al. 2009), which used a seed-based functional connectivity analysis in breast cancer patients following chemotherapy, showed a decrement in the connectivity of the posterior cingulate cortex and the intraparietal sulcus. Importantly, the posterior cingulate cortex is a central node to the Default Mode Network (DMN). DMN is one of the most observed resting state networks (RSNs) that is usually engaged when subjects are not focused on cognitive processes coming from the external environment or when they are processing internal focused tasks. DMN is localized in the posterior cingulate cortex, precuneus, medial temporal, medial prefrontal and lateral parietal cortex (Buckner et al. 2008; Spreng and Schacter 2012). Another study, which used graph theoretical analysis (Bruno et al. 2012), displayed altered global brain network organization consisting in a significant decrement of global clustering and a disruption of the regional DMN network characteristics in frontal, striatal and temporal areas in breast cancer patients. In addition, Kesler and colleagues (Kesler et al. 2013), used multivariate pattern analysis (MVPA) to classify profiles of DMN functional connectivity. Results showed disrupted DMN connectivity in those patients treated with chemotherapy, as well as an accurate classification performance using the connectivity pattern as the input of the classifier, except for the classification between cancer patients before chemotherapy and healthy subjects. Thus, as shown by the studies described above, there are several methods to analyze RS-fMRI data (Lee et al. 2013).

There is, however, another extensively used approach to assess functional connectivity called Independent Component Analysis (ICA). ICA is a multivariate statistical technique that estimates functionally related networks by maximization of independence among components (Lee et al. 2013). ICA has become a successful data-driven and model free analysis tool (Abou-Elseoud et al. 2010; De Luca et al. 2006). These characteristics, in contrast to previously mentioned methods, are important because a priori specification of a seed region or region of interest (ROI) to perform ICA analyses is not needed. It estimates functional connectivity of spatially distributed brain regions, from the blood-oxygen-level dependent response fluctuations of resting or active brain (Smith et al. 2009). Interestingly ICA has only been used to assess connectivity brain changes in cancer population in a recent study (Hampson et al. 2015) focused on cancer-related fatigue.

To date, most investigations on treatment and cancer-related cognitive changes have focused on breast cancer patients. Cancer and chemotherapy-related cognitive research focused on lung cancer population has been scarce. Early studies found that non-small cell lung cancer (NSCLC) patients exhibited transient cognitive deficits soon after chemotherapy treatment (Kaasa et al. 1988a; b). Other studies, focusing exclusively on small-cell lung cancer (SCLC) patients, found that nearly 60–90% of patients were cognitively impaired 1 to 5 months after concluding chemotherapy (Grosshans et al. 2008; Komaki et al. 1995). Additionally, to the best of our knowledge, only three studies have examined the structural and functional neural changes following chemotherapy treatment in lung cancer population (Horky et al. 2014; Simo et al. 2015; Simo et al. 2016a). Two of these previous studies, conducted in the same cohort of lung cancer patients examined in the present study, showed gray and white matter structural damage mostly focused in bilateral temporal regions of SCLC (Simo et al. 2015; Simo et al. 2016a). Thus, the study of the toxic effects of cancer and chemotherapy on cognition in this population remains challenging and underrepresented in the literature.

The present study aimed to investigate the cancer- and chemotherapy-related differences in RS-fMRI using an ICA analysis. Based on previous structural neuroimaging findings, we hypothesized that both DMN but also temporal networks will be functionally disrupted in the lung cancer population. We explored differences in functional connectivity of brain networks between three gender-, age- and education-matched groups: SCLC patients one month following chemotherapy (C+), NSCLC patients prior to chemotherapy (C-), and a healthy control (HC) group.

## Methods

### Patients

Patients were prospectively recruited between December 2010 and December 2013 from the Lung Cancer Unit-ICO L'Hospitalet ($n$ = 26) and the Radiation Oncology Department-ICO Badalona-Hospital Germans Trias i Pujol ($n$ = 4). Patients were eligible if they had an histologically proven diagnosis of either NSCLC or SCLC, were between the ages of 40 and 70 years, had no severe concomitant systemic illness or psychiatric disorder with a negative impact on cognitive function, or had no contraindication to undergo MRI. Patients were excluded if they had evidence of brain metastases on MRI. This cross-sectional analysis is a part of a longitudinal study designed to examine the effects of prophylactic cranial irradiation (PCI) in SCLC patients (Simo et al. 2015; Simo et al. 2016b). C+ ($n$ = 15) who were eligible to receive PCI and were anti-HU negative were enrolled one month following completion of chemotherapy and prior to PCI. C- ($n$ = 15) who were eligible to receive a platinum-based chemotherapy were enrolled in the study before the initiation of chemotherapy. The NSCLC group was selected as control for the evaluation of chemotherapy effects on SCLC patients because NSCLC patients presented common organ location, had similar demographic and clinical features, and underwent the same platinum-based chemotherapy without PCI. Gender, age and education-matched HC ($n$ = 15) who met the same inclusion (except for cancer diagnosis) and exclusion criteria were recruited through community advertisements. Vascular risk factors were collected and classified in low-risk (if the patient had none or one risk factor) and high-risk (if the patient had two or more risk factors) groups (Welzel et al. 2008). The study protocol was approved by the local Ethical Commission and written informed consent was obtained from all participants.

### Neuropsychological assessment

Patients were evaluated using: Mattis Dementia Rating Scale–2 (MDRS-2); selected subtests of the Spanish version of the Wechsler Adult Intelligence Scale-III (Vocabulary; Information; Similarities; Digit Span; Letter Number Sequencing; Block Design; Matrix Reasoning; Picture Completion); Rey Auditory Verbal Learning Test (RAVLT); Wechsler Memory Scale–III Logical Memory I-II; Rey-Osterreith Complex Figure Test Copy, Immediate and Delayed; Spanish Version of the Boston Naming Test; Verbal Fluency test (Phonemic and Semantic); Trail Making Test (A-B); and Beck Depression Inventory (BDI). Intelligence quotient was estimated using Vocabulary performance. Raw cognitive test scores were compared with the validated Spanish normative values, corrected for age and education, and converted into z-scores. Neuropsychological results are reported uncorrected for multiple testing and Bonferroni corrected for multiple cognitive testing ($n$ = 22). Cognitive impairment was defined as a MDRS-2 raw score less than 123 (Mattis 1988), one test ≥2 or two tests ≥1.5 standard deviations below the sample mean (Correa et al. 2013). All statistical analyses were conducted in SPSS 18.0 (SPSS, Chicago, IL). One-way analysis of variance and Chi-square tests were used to test group differences with a critical $p$-threshold of 0.05.

### Estimation of resting state networks

#### *MRI scans acquisition*

Participants' images were acquired in 3 Tesla MRI (Siemens Magnetom Trio Tim SyngoB17). Functional images were obtained using a single-shot T2*-weighted gradient-echo echo-planar imaging sequence [slice thickness = 4 mm; no gap; number of slices =32, order of acquisition interleaved; repetition time (TR) = 2000 ms; echo time (TE) = 29 ms; flip angle 80°; matrix 128 × 128; field of view (FOV) = 240 mm; voxel size 1.87 mm × 1.87 mm × 4 mm]. Each slice was aligned to the plane intersecting the anterior and posterior commissures. In addition to the functional images, a high-resolution T1-weighted image was obtained for each subject using a magnetization-prepared rapid-acquired gradient echo sequence [MPRAGE; slice thickness = 1 mm; no gap; number of slices =240; TR = 2300 ms; TE = 2.98 ms; matrix =256 × 256; FOV = 244 mm]. Functional MRI data were acquired while participants were resting in the scanner with their eyes closed during 7 min and 14 s.

#### *Preprocessing*

Data was preprocessed using Statistical Parameter Mapping software (SPM8, Wellcome Department of Imaging Neuroscience, University College, London, UK, http://www.fil.ion.ucl.ac.uk/spm/). After Slice Timing, all images were realigned and their mean image was calculated. The structural T1 images were coregistered to their respective mean functional image and segmented using the New Segment toolbox included in SPM8. Following segmentation, grey and white matter images were fed to DARTEL in order to achieve normalization (Ashburner 2007). After normalization, data was subsampled to 2 $mm^3$ (91 × 109 × 91 voxels) and spatially smoothed with an 8 mm at full width at half maximum (FWHM) Gaussian kernel.

#### *Independent component analysis*

**Independent component analysis general parameters** To extract the different functional networks by means of ICA, we used the GIFT software (http://icatb.sourceforge.net/) (Calhoun et al. 2001). Thus, the smoothed functional images

of subjects for each group independently (C+, C- and HC) and for the total sample were fed to GIFT. Before starting the analysis, it is necessary to set how many independents components (IC; i.e., RSNs) would be extracted (it is explained further in the text). ICA started with an intensity normalization step. After this first step, data was first concatenated and reduced to different temporal dimensions using principal component analysis, to be then analyzed with the Infomax algorithm (Bell and Sejnowski 1995). No scaling was used, as with the intensity normalization step, the intensities of the spatial maps obtained are already in percentage of signal change.

**The ICASSO algorithm** Most ICA algorithms, including the Infomax algorithm used in our study, are based on gradient methods using a cost function that must be minimized to reach a good estimation of ICs. There is a random initialization of parameters each time the procedure is executed. Consequently, these initial conditions can produce different results, in some cases giving local minima of the cost function (i.e., a more or less distant result of the expected better estimation). For this reason, it is recommended to repeat the ICA several times to calculate a reliability measure between the different results achieved. In addition, ICA depends on the number of ICs prefixed to run the analysis. For example, when too few ICs are calculated, the RSNs retrieved are not accurate enough (Abou-Elseoud et al. 2010), but if too much ICs are calculated then some redundancies, namely two or more RSNs imprecisely overlapping each other, may appear in the results. For this reason, in order to ensure the best RSNs estimation, this reliability analysis is equally recommended (Himberg et al. 2004).

The ICASSO software package included in the GIFT toolbox executes these reliability calculations. This algorithm includes an objective quality index ($I_q$), based on clustering of mutual similarities between the different estimated components of the set of runs of ICA, that reflects the compactness and isolation of a cluster (Himberg et al. 2004). After all, this algorithm gives the best possible result based on the centrotype achieved after clustering the obtained components from the different runs. Finally there is a back-reconstruction process from the group ICA components estimated to the individual activation values for each participant of the different groups and for each component. This result consists of an individual map for each participant.

**Resting state networks visual identification** Once the ICA is performed, it is fundamental to carry out a correct visual identification of the RSNs extracted. For this reason, four one-sample t-tests of the individual spatial maps of each of the independent components (IC) estimated were calculated, one for the Total Sample and three for the groups taken separately (C+, C- and HC). To make these calculations, each subject's network was treated as a random effect (Calhoun et al. 2001). Once we had the aforementioned t-maps of each IC, we made the visual identification of the RSNs. We used a critical threshold with $p \leq 0.05$ (family wise error correction, FWE) for the total sample ($n = 45$) and a critical threshold with $p < 0.001$ (uncorrected) for each group separately ($n = 15$). It was considered that a RSN was correctly extracted if it appeared both in the total sample and in each group (C+, C- and HC) separately.

The selection of the most reliable number of ICs to extract was performed using a two steps procedure. During the first step, we performed in an exploratory way 100 repetitions of the ICA using the ICASSO procedure with the number of extracted ICs set to 10, 15, 20, 25 and 30 for the total sample and for each one of the three groups separately to ensure the best possible results. RSNs were identified by visual inspection and we found that the best extracted RSNs appeared for 15 and 20 ICs. The lower value (15 IC) was the model order that gave the higher number of large-scale RSNs (i.e., of recognizable networks), a result that is in agreement with previous literature (Abou-Elseoud et al. 2010), without redundancies for the total sample and for each one of the three groups separately. The upper value (20 IC) was the first analysis in which redundancies begun to appear.

During the second step, ICA analysis was performed 100 times using the ICASSO procedure with IC fixed from 15 to 19 IC. After visual inspection, we identified different well-known RSNs that will be reported in the Results section. To ensure enough goodness of fit of this procedure we performed an inter-rater reliability analysis (Franco et al. 2009) of the RSNs identification process using the Cohen's Kappa Coefficient (Cohen 1960). Once we had finished this procedure we had different RSNs that, in some cases, were extracted for different IC values. Then, the definitive number of ICs was selected based on the objective quality index $I_q$. When a RSN appeared for more than one IC value, then the number of fixed ICs that maximized the mean $I_q$ parameter of the different groups (C+, C- and HC) was selected as the one to be set to the second level group analyses. As aforementioned, the greater the value of $I_q$ the greater the reliability of the result achieved. See Fig. 1.

*Statistical analysis between groups*

The individual maps of the RSNs selected for each group member were the ones used for the statistical analyses. A mask was calculated for all the RSN identified using the one sample t-test for the total sample with critical $p \leq 0.05$ (FWE). Only voxels included in these masks were analyzed. Then, for each RSN identified with the procedure described above, a one-way Analysis of Variance (ANOVA) with three levels (HC, C+, and C-) was calculated to find differences between

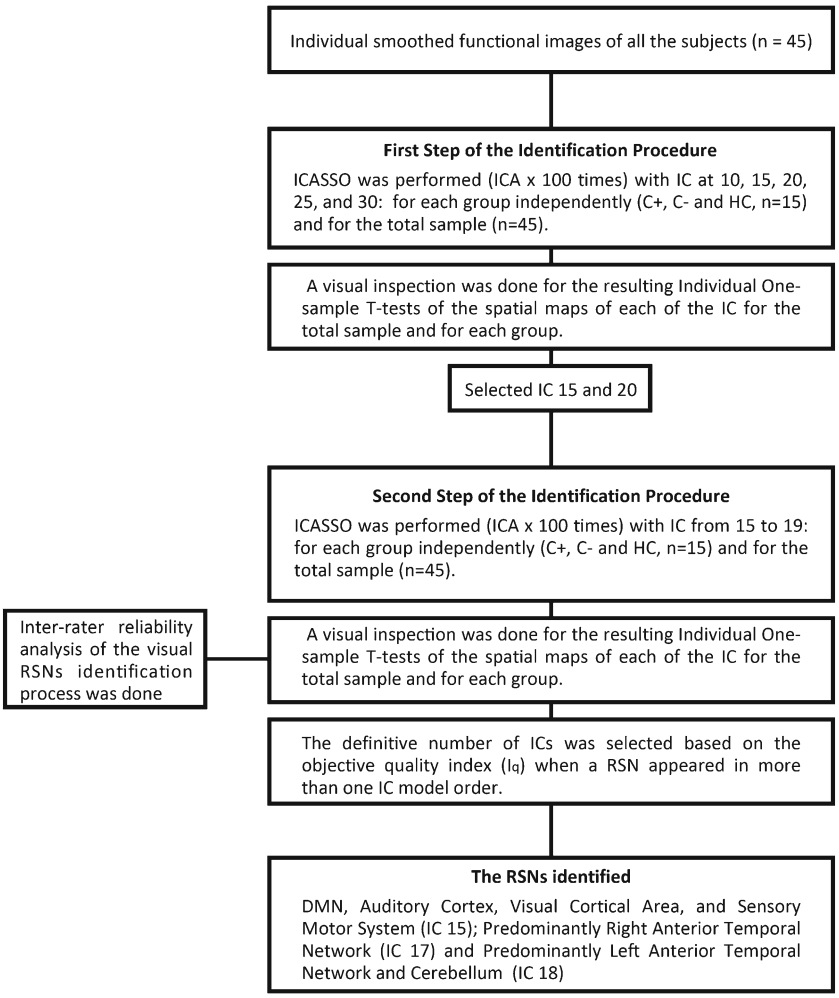


**Fig. 1** Flowchart of the identification progress of Resting State Networks

groups. Additional post-hoc analyses using two-sample t-tests were performed to show the directions of the significant differences found between groups FWE-corrected at the voxel level. A Bonferroni correction was also performed to correct for multiple comparisons of the RSNs identified.

Additionally, for each of the RSN showing group differences, and concretely for the patient's groups involved in these comparisons, a Region of Interest (ROI) for each significant cluster peak was defined (sphere of 4 mm of radius from the peak) and it was then applied to each individual image. Again, for each RSN of interest, a mean voxels' activation value for each individual and each ROI was obtained. We then used these voxels' activation values to make an exploratory analysis of the association between cognitive deterioration and brain connectivity changes, by computing a Point Biserial correlation coefficient analysis (Tate 1954) between cognitive impaired and not cognitive impaired patients and the individual mean of the voxel activation values of each ROI defined. More concretely, a Point Biserial correlation analysis was performed between all the ROIs created at the significant peaks of the different RSN and cognitive impairment (yes/no).

## Multivariate pattern analysis

MVPA was carried out with the Pattern Recognition for Neuroimaging Toolbox v1.1 (http://www.mlnl.cs.ucl.ac.uk/pronto/prtsoftware.html, (Schrouff et al. 2013). There are two Machine Learning (ML) algorithms implemented in this toolbox, the Support Vector Machines (SVM) and the Gaussian Process Classification (GPC) algorithm. These algorithms were developed to deal with classification problems. SVM separates between classes projecting a low dimensional training data where it is difficult to perform a linear separation between classes, into a higher dimensional feature space where it is easier to find a hyperplane to linearly separate patterns. In contrast, GPC based on Bayesian Theory, uses its rules to find a function distribution that approximates the best possible training set classification. SVM has been widely used to perform MVPA (Mourao-Miranda et al. 2005) but there are some examples of GPC applied to MVPA (Challis et al. 2015; Marquand et al. 2010). We tested both MPVA approaches and we found a better performance of GPC in front of SVM in our data. Each feature set was constructed

using the scans of the RSNs that showed significant differences in the previous step for each one of the groups' combinations. Specifically, a mask defined with the significant clusters of the comparisons between groups for each RSN was applied to the scans. Values from all voxels within the mask were used. Features were mean centered, and cross-validation was performed leaving one subject out per group. Estimation of the average and groups' classification accuracy and signification was performed by a permutation test of 10,000 iterations. MVPA gives the discriminant performance achieved as a balanced accuracy of the different groups to be classified and classification accuracy for each group independently.

Binary classification accuracy assessment can be performed using Receiver Operating Characteristic (ROC) curves. The ROC curve is the result of plotting sensitivity, against the complement of specificity (1-specificity) of the classification process. The Area Under the Curve (AUC) given by the plot is an indicator of the accuracy of binary decision-making processes (Fawcett 2006). The AUC of the ROC was calculated to show the categorization power in terms of sensitivity and specificity. All ROC analyses were conducted in SPSS 21.0 (SPSS, Armonk, NY).

## Results

### Patient characteristics

Characteristics of the entire cohort are described in Table 1. There were no significant differences between groups in age, gender, education or grouped vascular risk factors. When analyzed independently, only smoking history showed a significant difference between lung cancer patients and HC ($X^2$ (1, Yates continuity correction) = 10,04, $p < 0.002$), but no differences were observed between both cancer groups (C+ and C-, Fisher exact test, $p > 0.48$).

### Neuropsychological assessment

The neuropsychological assessment revealed that lung cancer patients performed significantly worse than healthy controls in several subtests (WAIS-III Matrix Reasoning, WAIS-III Picture Completion, Wechsler Memory Scale -III Logical Memory I, Wechsler Memory Scale-III Logical Memory II, ROCF immediate copy and Phonemic fluency). However, after applying Bonferroni correction, only ROCF immediate copy resulted significant between C+ and HC groups ($p < 0.002$). Both cancer groups exhibited a significant higher rate of cognitive impairment (40% of C+ and 40% of C-) compared to healthy controls ($X^2$ (1, Yates continuity correction) = 6,26, $p = 0.012$). See Table 2.

### Resting state networks

#### *Networks identified*

The inter-rater reliability estimation resulted in a good agreement between raters (Cohen's Kappa Coefficient 0.62; 95% CI, 0.534 to 0.703; $p < 0.0001$) (Altman 1999). The RSNs identified with ICA with a model order of 15 components were: the DMN, and other classical networks localized in Auditory Cortex, Visual Cortical Area, and Sensory Motor System (see Fig. 2) (Beckmann et al. 2005). Predominantly Right Anterior Temporal Network (RAT) was detected with a model order of 17 components (Kiviniemi et al. 2009). Finally, Predominantly Left Anterior Temporal Network (LAT) and Cerebellum (Cb) appeared when the number of predefined components was 18. Other RSNs were discarded for several reasons: in some cases, they were artifacts, redundancies or they didn't meet the eligible criteria stated above (Table 3).

#### *Differences between groups*

We found significant differences between groups in four of the seven RSN identified. These differences appeared in DMN, LAT, RAT and Cb. The DMN showed a decreased connectivity in both lung cancer groups compared to HC (precuneus and middle occipital gyrus bilaterally). Specifically, the C+ group showed decreased connectivity compared to HC in left cuneus and in precuneus and middle occipital gyrus bilaterally. The C- group showed decreased connectivity compared to HC in bilateral precuneus, right middle temporal gyrus, posterior cingulate gyrus and left inferior parietal and middle occipital gyrus. In addition, the C+ group showed decreased connectivity of the DMN compared to C- in left cuneus (see Fig. 3).

Significant differences in the Left Anterior Temporal network (LAT) consisted in increased connectivity of both lung cancer groups compared with HC and of the C+ group compared to HC in the left Inferior Temporal Gyrus. Similarly, in the Right Anterior Temporal network (RAT) there was an increased connectivity of both lung cancer groups compared to HC and of the C+ group compared to HC in right parahippocampal gyrus, and of the C+ group compared to C- in right inferior temporal gyrus and middle temporal pole (see Fig. 3).

We also found differences in the cerebellum network (Cb) consisting in increased connectivity of the C+ group compared to HC (vermis and left superior cerebellum) and the C- group compared to HC (inferior cerebellum bilaterally). See Table 4 and Fig. 3.

Point biserial correlation analyses showed a marginal relationship between cognitive impairment and the mean functional connectivity in Left Cuneus (MNI -2, −28, 26) within

**Table 1** Baseline demographics and vascular risk factors of the entire cohort

| | C+ ($n$ = 15) | C- ($n$ = 15) | HC ($n$ = 15) | *p-value* |
|---|---|---|---|---|
| Age (years)* | 59.73 ± 6.92 | 60.07 ± 6.69 | 59.80 ± 7.55 | 0.99 |
| Gender[&] | | | | |
| Male | 13 (87) | 13 (87) | 13 (87) | 1 |
| Female | 2 (13) | 2 (13) | 2 (13) | |
| Education (years) ** | 8 (0,17) | 8 (0,12) | 7 (6,19) | 0.98 |
| Estimated verbal IQ* | 9.92 (2.43) | 10.31 (3.07) | 12 (2.88) | 0.09 |
| Smoking[&] | 15 (100) | 13 (87) | 7 (47) | **0.002** |
| Alcohol[&] | 7 (47) | 2 (13) | 3 (80) | 0.72 |
| HT[&] | 6 (40) | 9 (60) | 4 (27) | 0.18 |
| DM type II[&] | 2 (13) | 6 (40) | 1 (7) | 0.23 |
| Dyslipidemia[&] | 6 (40) | 8 (53) | 10 (67) | 0.34 |
| Vascular risk factors[&] | | | | |
| Low-risk (0 or 1) | 6 (40) | 4 (27) | 7 (47) | 0.52 |
| High-risk (≥ 2) | 9 (60) | 11 (73) | 8 (53) | |

Statistically significant results are marked in bold; C+ chemotherapy-treated small-cell lung cancer group; C- non-chemotherapy treated non-small cell lung cancer group; *HC* healthy control group; *IQ* Intelligence quotient; *HT* hypertension; *DM* diabetes mellitus

*(mean ± SD)

**median (range)

[&] *n* (%)

the DMN. Concretely we found a significant correlation ($r = -0.546$, $p = 0.035$, uncorrected for multiple comparisons) for the C+ patients group. The lower the mean functional connectivity in the DMN, the higher the rate of cognitive impairment for the C+ group.

*Classification accuracy using multivariate pattern analysis*

Classification performance of our resulting RSNs significant t-maps for all comparisons was highly accurate (see Fig. 4). The GPC was more accurate than the SVM classification for all the comparisons, for this reason the results reported come from the GPC algorithm. Specifically, balanced accuracy for lung cancer (grouping C+ & C-) and HC group was 82.2% (AUC 0.82, $p < 0.001$), being for lung cancer 91.1% ($p < 0.011$) and for HC 73.3% ($p < 0.001$) independently; between C+ and HC groups reached a balanced accuracy of 95.8% (AUC 0.96, $p < 0.001$), being in C+ of 93.3% ($p < 0.001$) and in HC of 98.3% ($p < 0.001$) independently; between C- and HC groups was 86.7% (AUC 0.87, $p < 0.001$), being for C- of 83.3% ($p < 0.002$) and for HC of 90.0% ($p < 0.001$); between C+ and C- group reached accuracy was 86.7% (AUC 0.87, $p < 0.001$), being for C+ group of 80.0% ($p < 0.001$) and for C- group of 93.3% ($p < 0.001$); and finally, classification between the three groups independently (C+, C- and HC) reached a balanced accuracy of 78.9% ($p < 0.001$), being for C+ group of 78.3% ($p = 0.011$), for C- group of 71.7% ($p = 0.024$) and for HC group of 86.7% ($p < 0.001$).

## Discussion

The present study documents brain connectivity differences in a cohort of lung cancer patients. As an improvement from previous studies, selection of RSNs was based on the ICASSO algorithm to ensure that our results were as much reliable as possible, being our study, to the best of our knowledge, the first to use this algorithm in chemobrain literature. Additionally, we used the objective quality index $I_q$ to emphasize the importance of achieving the most possible reliable and qualitative RSNs previously to the analysis of statistical differences between groups. Our results revealed that lung cancer patients, both C+ and C- groups, exhibited cognitive impairment together with differences in connectivity in DMN, LAT, RAT and Cerebellum. Concretely we found decreased connectivity of the posterior regions of the DMN and increased connectivity in bilateral temporal and cerebellar regions in comparison to the HC group. Additionally, the C+ group displayed brain-specific differences in comparison to the C- group. The C+ group exhibited decreased connectivity in left cuneus and increased connectivity in right inferior temporal gyrus and middle temporal pole in comparison to C- group. Hence, these connectivity-imaging findings suggest that both cancer by itself and platinum-based chemotherapy might be associated with the development of cognitive toxicity.

The DMN, one of the most commonly observed RSNs, includes the precuneus, posterior cingulate, medial frontal, middle temporal, and lateral parietal regions as well as the hippocampus (Damoiseaux et al. 2006) and supports

**Table 2** Neuropsychological results

| | C+ ($n$ = 15) | C- ($n$ = 15) | HC ($n$ = 15) | *One-way ANOVA p-value* ¤ |
|---|---|---|---|---|
| Cognitive impairment[&] | **6 (40)**$^{+}$ | **6 (40)**$^{++}$ | 0 (0) | **0.012**[a] |
| MDRS-2 [$] [**] | 144 (137–144) | 144 (134–144) | 144 (137–144) | 0.72[b] |
| BDI** | 11 (2–22) | 7 (2–27) | 5 (1–22) | 0.5[b] |
| WAIS-III Vocabulary* | -0.03 (0.81) | 0.10 (1.02) | 0.67 (0.96) | 0.09 |
| WAIS-III Information* | 0.23 (0.86) | 0.46 (1.12) | 0.89 (0.96) | 0.18 |
| WAIS-III Similarities* | 0.38 (0.80) | 0.41 (1.11) | 0.60 (0.75) | 0.58 |
| WAIS-III Digits span* | 0.23 (1.06) | 0.20 (0.99) | 0.47 (0.90) | 0.53 |
| WAIS-III Letters Number Sequencing * | -0.20 (0.88) | 0.02 (0.89) | 0.29 (0.77) | 0.23 |
| WAIS-III Block Design* | 0.13 (0.99) | 0.49 (0.97) | 0.75 (0.83) | 0.09 |
| WAIS-III Matrix Reasoning* | **-0.38 (0.84)**$^{+}$ | **-0.08 (1.19)**$^{++}$ | 0.64 (0.87) | **0.01** |
| WAIS-III Picture Completion* | **1.38 (0.69)**$^{+}$ | 2.28 (0.79) | 1.95 (1.02) | **0.04** |
| RAVLT raw 1[$] | 4.15 (1.62) | 4.46 (1.50) | 5.20 (1.65) | 0.15 |
| RAVLT long-delay recall (A7)[$] | 6.15 (3.08) | 7.31 (3.01) | 8.00 (3.02) | 0.30 |
| RAVLT list B[$] | 4.69 (1.54) | 4.62 (2.22) | 5.20 (1.37) | 0.42 |
| RAVLT short-delay recall (A6) [$] | 6.00 (2.55) | 6.62 (3.35) | 8.00 (3.02) | 0.16 |
| RAVLT long-delay recognition[$] | 10.15 (2.30) | 11 (2.86) | 11.80 (2.04) | 0.18 |
| WMS-III Logical Memory I* | 0.20 (0.77) | -0.18 (0.75) | 0.60 (0.95) | 0.07 |
| WMS-III Logical Memory II * | 0.79 (1) | **0.02 (0.79)**$^{+++}$ | 0.95 (1.09) | **0.02** |
| ROCF immediate copy* | **0.46 (0.81)**$^{+}$ | 1.59 (1.18) | 1.82 (1.07) | **0.001**© |
| ROCF delayed copy* | 0.69 (0.64) | 0.46 (0.74) | 0.71 (0.68) | 0.45 |
| Brief Spanish version Boston Naming Test* | 0.79 (0.70) | 0.64 (0.90) | 0.49 (0.50) | 0.39 |
| Animal naming* | 0.36 (0.76) | 0.13 (0.64) | 0.18 (0.77) | 0.51 |
| Phonemic fluency* | **-0.26 (1.25)**$^{+}$ | -0.28 (1.03) | 0.53 (0.65) | **0.03** |
| Trail Making test A* | -0.28 (0.56) | -0.28 (0.78) | 0.20 (0.93) | 0.22 |
| Trail Making test B* | -0.54 (0.76) | -0.56 (0.77) | -0.07 (0.84) | 0.22 |

All results are z-scores except for [$] raw score

C+: chemotherapy-treated small-cell lung cancer group; C-: non-chemotherapy treated non-small cell lung cancer group; *HC* Healthy control group. MDRS-2: Mattis Dementia Rating Scale-2; *RAVLT* Rey Auditory-verbal Learning Test; *WMS-III* Wechsler Memory Scale – III; *ROCF* Rey-Osterreith Complex Figure; *BDI* Beck Depression Inventory

+ C+ performed significantly worse than HC; ++ C- performed significantly worse than HC; +++ C- performed significantly worse than HC and C+

*Statistically significant results are marked in bold; P*-values are reported uncorrected for multiple comparisons. Between-group differences that were significant after Bonferroni correction are marked with ©

* mean (SD); [&] $n$ (%); ** median (range)

¤ Between-group ANOVA $p$-value, except from [a] (Chi-Square) and [b] (Kruskal-Wallis test). T-test was used to compare pairs of groups

important core processes such as implicit learning, autobiographical memory retrieval, prospection, monitoring, and other internally focused thought processes (Raichle 2011). The DMN connectivity reduction has been described as a promising biomarker of brain aging, mild cognitive impairment and Alzheimer's disease (Damoiseaux 2012; Sheline et al. 2010). Concerning DMN connectivity and chemotherapy, previous RS-fMRI studies in line with our findings in lung cancer patients, showed a decrement in global DMN connectivity with special emphasis in the posterior cingulate cortex, the intraparietal sulcus and the precuneus (Bruno et al. 2012; Dumas et al. 2013; Kesler et al. 2013) (LaViolette et al. 2009; Piccirillo et al. 2015). Concretely, in our study although both lung cancer groups, prior and following chemotherapy, exhibited a global DMN disruption, those changes were larger for the C+ group. In contrast to breast cancer population, lung cancer patients underwent platinum-based chemotherapy, which as described in animal studies, is associated with an increased cell death and decreased cell division in the subventricular zone, the dentate gyrus of the hippocampus and in the corpus callosum (Dietrich et al. 2006). Taken together, our findings suggest that the cancer by itself might be responsible for most of the DMN connectivity disruption observed in lung cancer patients and that the addition of platinum-based chemotherapy adds modest but brain-specific changes.

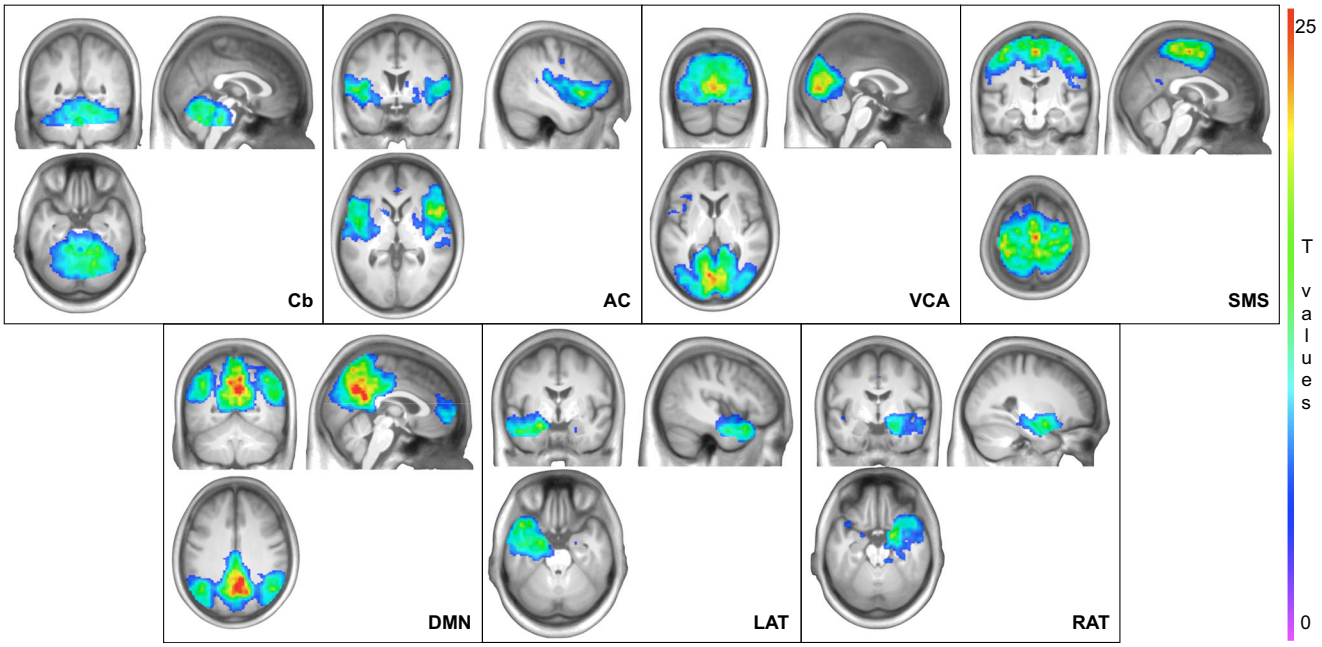


**Fig. 2** Resting State Networks identified using Independent Component Analysis for the total sample ($n$ = 45). The networks identified are Cerebellum (Cb), Auditory Cortex (AC), Visual Cortical Area (VCA), Sensory Motor System (SMS), Default Mode Network (DMN), Predominantly Left Anterior Temporal Network (LAT) and Predominantly Right Anterior Temporal Network (RAT). The maps are significant using athreshold of $p \leq 0{,}05$ (Family-wise Error Correction) and a cluster extent of 100 voxels. Results are displayed on a t-map and superimposed on a customized T1 template created averaging the warped images after normalization. The threshold bar shown at the right side of the figure represents the one-sample t-test values

Less studied, but also very important, are the anterior temporal networks. Specifically, the lateral anterior temporal network includes superior, middle and inferior temporal gyrus and the medial anterior temporal network includes the parahippocampal gyrus and the uncus involving the head of the hippocampus and the amygdala (Gour et al. 2011). Functionally, the different components of these temporal networks have been involved in declarative memory (Eichenbaum et al. 2007). Recently, an increased connectivity of these networks has been described in patients with cognitive impairment (Gour et al. 2011). In the present study, both lung cancer patients revealed increased connectivity of bilateral temporal networks in comparison to HC, but also increased connectivity of the C+ group compared to C- in right inferior temporal gyrus and middle temporal pole. Although both bilateral temporal networks showed increased connectivity in both lung cancer groups, this increment was higher in C+ compared to C- in brain specific regions, similarly to our findings in the DMN. In our opinion, the increased connectivity of bilateral temporal networks may be compensatory in nature, as it has been described in mild cognitive impaired population (Gour et al. 2011).

Additionally, we also found differences in the Cerebellum network consisting in increased connectivity of the C+ group compared to HC (vermis and left superior cerebellum) and the C- group compared to HC (inferior cerebellum bilaterally). The cerebellum processes information from functionally diverse regions of the cerebral cortex; however, the topography of the connections between the cerebellar and cerebral cortices

**Table 3** $I_q$ value criterion for Resting State Networks selection

| | Number of components | | | | |
|---|---|---|---|---|---|
| | 15 | 16 | 17 | 18 | 19 |
| Cerebellum | 0,9782 | 0,9787 | 0,9801 | 0,9812* | 0,9800 |
| Auditory cortex | 0,9848* | 0,9776 | 0,9813 | 0,9823 | 0,9799 |
| Visual cortical area | 0,9806* | 0,9748 | 0,9782 | 0,9795 | 0,9796 |
| Default mode network | 0,9795* | 0,9434 | 0,9715 | 0,9711 | 0,9779 |
| Sensory motor system | 0,9852* | 0,9717 | 0,9831 | 0,9827 | 0,9743 |
| Predominantly left temporal | 0,9769 | 0,9769 | 0,9760 | 0,9770* | 0,9733 |
| Predominantly right temporal | NP | 0,9747 | 0,9761* | NP | NP |

*Maximum $I_q$, *NP* Not present

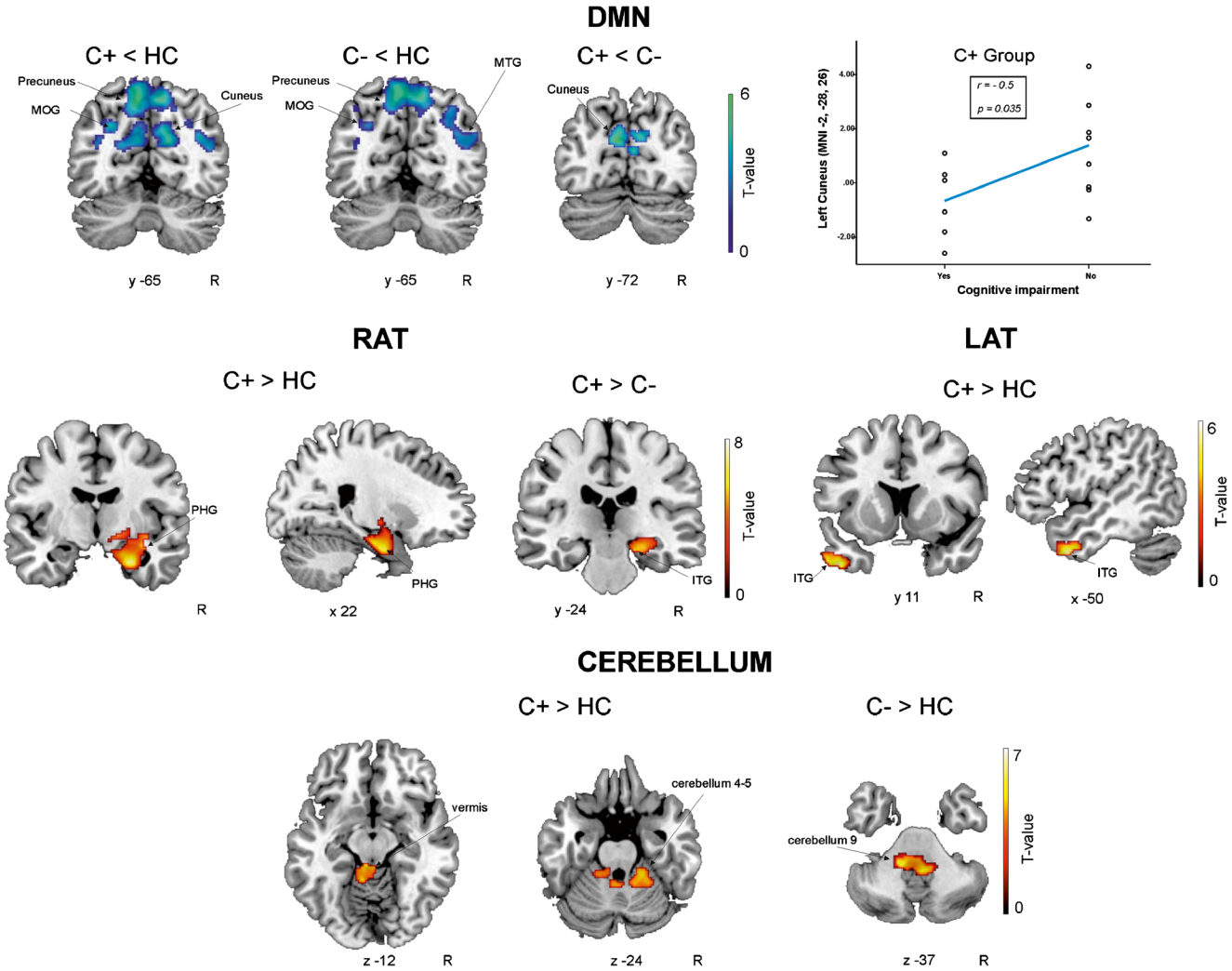


**Fig. 3** Group differences for functional connectivity between groups. Significant differences between groups are reported at a FWE-corrected threshold at voxel level but displayed on a t-map and superimposed on a standardized T1 template using MNI coordinates at an uncorrected $p$ 0.001 with a cluster extent of 20 voxels. Clusters in blue show a decrease of the functional connectivity and clusters in red show an increase of the functional connectivity of the patients groups (C+ or C-) against Healthy Controls. Point biserial correlation between cognitive impairment (Yes/No) and the mean functional connectivity in Left Cuneus (MNI -2, −28, 26) within the DMN for the C+ group showed a significant correlation. C+ Lung Cancer Patients following Chemotherapy; C- Lung Cancer Patients before Chemotherapy; HC healthy control group; R: right hemisphere; MOG-Middle Occipital Gyrus; MTG-Middle Temporal Gyrus; PHG-Parahippocampal Gyrus; ITG-Inferior Temporal Gyrus. The threshold bar shown at the right side of the figure represents the one-sample t-test values

remains largely unmapped (Duzel et al. 2009; O'Reilly et al. 2010). A recent study exploring RSNs found that cerebellum can be functionally divided in zones: a primary sensorimotor area, functionally connected to primary sensory and motor cortex, and what we might name as a supramodal zone, functionally connected to dorsolateral prefrontal and inferior posterior-parietal regions (O'Reilly et al. 2010). In our study, while the C+ group showed an increased connectivity of superior cerebellum more functionally connected to primary sensory-motor cortex, the C- group showed a bilateral increased connectivity of a part of the inferior cerebellum included in the functionally described supramodal zone that might assist cortical brain regions in their aim to compensate cognitive deficits.

More important is the relationship between functional and structural brain changes associated with chemotherapy-induced cognitive impairment. Our group recently published a structural MRI study with the same lung cancer cohort (Simo et al. 2015). This study showed gray matter atrophy in bilateral paralimbic regions including the cingulate cortex, the insula, the parahippocampal gyrus and left thalamus together with white matter integrity damage in bilateral inferior longitudinal fasciculus - which connects temporal regions with parietooccipital ones - of the C+ group. Supplementary Fig. 1 depicts the overlap of past and current results. In the same vein, previous studies focusing in mild cognitive impaired population found that gray matter atrophy was related to a decrease in DMN connectivity

**Table 4** Localization of pairwise significant differences found at different Resting State Networks

| Contrast | Peak MNI coordinates | Cluster extent | Peak student t | Peak p (FWE) | Cluster localization |
|---|---|---|---|---|---|
| Cerebellum | | | | | |
| C+ > HC | 4–30 -14 | 39 | 7,01 | $P < 0,001$ | Vermis |
| | −12 -26-16 | 24 | 6,07 | $P < 0,002$ | Left cerebellum 3 |
| C- > HC | 14–40 -40 | 28 | 6,58 | $P < 0,001$ | Right cerebellum 9 |
| | −4 -46 -38 | 23 | 5,16 | $P < 0,014$ | Left cerebellum 9 |
| Default mode network | | | | | |
| C+ < HC | 8–70 54 | 390 | 7,22 | $P < 0,001$ | Right and left precuneus |
| | −38–76 28 | 104 | 6,68 | $P < 0,001$ | Left middle occipital gyrus |
| | 12–68 32 | 59 | 6,11 | $P < 0,001$ | Right precuneus |
| | 38–68 26 | 33 | 6,00 | $P < 0,001$ | Right middle occipital gyrus |
| | −2 -88 26 | 24 | 5,75 | $P < 0,001$ | Left cuneus |
| C- < HC | -6 -68 56 | 897 | 8,79 | $P < 0,001$ | Right and left precuneus |
| | −38–76 28 | 82 | 6,71 | $P < 0,001$ | Left middle occipital gyrus |
| | 8–34 46 | 21 | 6,09 | $P < 0,001$ | Posterior cingulate |
| | 42–68 24 | 21 | 5,47 | $P < 0,001$ | Right middle temporal gyrus |
| | −44 -48 46 | 23 | 5,43 | $P < 0,001$ | Left inferior parietal gyrus |
| C+ < C- | -8 -76 22 | 30 | 5,89 | $P < 0,001$ | Left cuneus |
| C+ & C- < HC | -6 -68 56 | 1061 | 8,75 | $P < 0,001$ | Right and left precuneus |
| | −38–76 28 | 214 | 7,77 | $P < 0,001$ | Left middle occipital gyrus |
| | 40–68 26 | 73 | 6,31 | $P < 0,001$ | Right middle occipital gyrus |
| Left anterior temporal | | | | | |
| C+ > HC | -46 8–38 | 118 | 6,76 | $P < 0,001$ | Left inferior temporal gyrus |
| C+ & C- > HC | -46 6–36 | 45 | 5,53 | $P < 0,003$ | Left inferior temporal gyrus |
| Right anterior temporal | | | | | |
| C+ > HC | 26–6 -28 | 493 | 8,69 | $P < 0,001$ | Right parahippocampal gyrus |
| C+ > C- | 56 12–28 | 47 | 5,18 | $P < 0,001$ | Right inferior temporal gyrus and right middle temporal pole |
| C+ & C- > HC | 14–18 -20 | 107 | 5,75 | $P < 0,001$ | Right parahippocampal gyrus |

*FWE* Family wise error correction; *MNI* Montreal neurological institute coordinates; C+ Chemotherapy-treated small-cell lung cancer group; C- Non-chemotherapy treated non-small cell lung cancer group; *HC* Healthy control group

(Dickerson et al. 2004; Sperling 2007), and to an increase in temporal functional connectivity (Gour et al. 2011). This temporal increased connectivity has been traditionally interpreted as a compensatory mechanism that occurs in response to an early pathological insult (Gour et al. 2014). It has been hypothesized that hyperconnectivity is an early consequence of brain injury and disease (early structural damage including white matter integrity damage) through increasing neural network response to competing demands, as for example, increasing anterior temporal lobe connectivity to preserve memory functioning. When a more advanced neural loss (sever structural damage) occurs, network recruitment might reach an upper threshold and after that non-returning point, no longer hyperconnectivity exists (Hillary et al. 2015).

Regarding cognitive deficits, more than one third of the patients (40%) in both lung cancer groups met criteria for cognitive impairment; however the neuropsychological profile was quite different. The C- group performed worse than HC and C+ in long-term verbal memory, as has been described in cancer patients before the initiation of therapy (Shilling et al. 2005; Wefel et al. 2004). Following treatment, and in line with previous literature (Jim et al. 2012), the C+ group performed worse than the HC group in visuospatial measures and verbal phonemic fluency. Although cognitive changes associated with either cancer or cancer treatment have been extensively recognized, the pathogenesis of these neurocognitive changes remains unclear. In this setting, several hypotheses have been proposed including the biology of cancer as well as common risk factors for the development of both cancer and mild cognitive changes in normal aging (Ahles and Saykin 2007). This last hypothesis is also supported by the similar functional connectivity changes found in the present study in comparison to mild cognitive impairment literature.

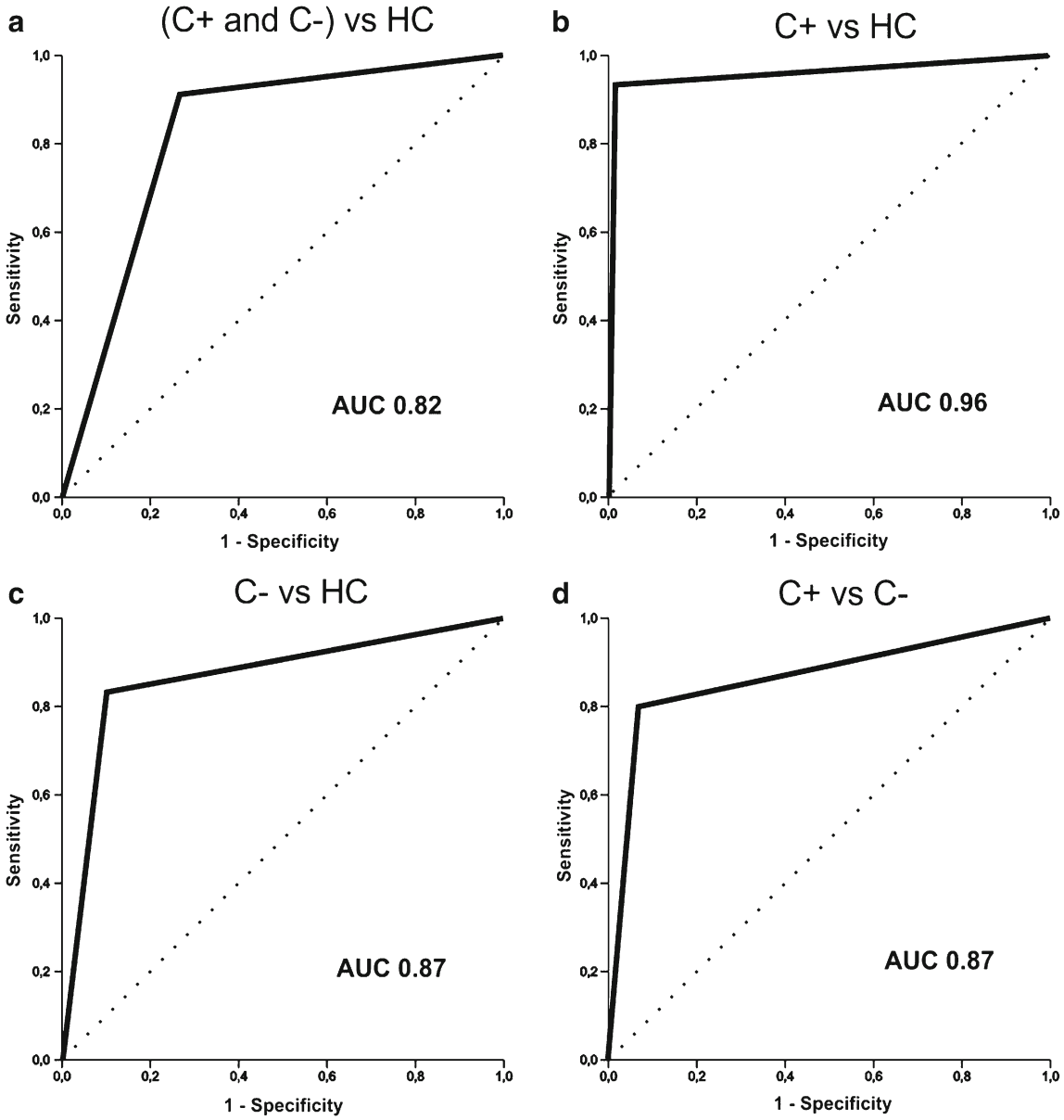


**Fig. 4** Receiver Operating Characteristic (ROC) Curves. Classification performance of the resulting RSNs significant T-maps for all comparisons balanced accuracy. **a** Lung cancer (grouping C+ & C-) and HC group (AUC 0.82, $p < 0.001$). **b** C+ and HC groups (AUC 0.96, $p < 0.001$). **c** C- and HC groups (AUC 0.87, $p < 0.001$). **d** C+ and C- group (AUC 0.87, $p < 0.001$)

Additionally, we found a significant correlation between cognitive functioning and connectivity changes in the DMN for the C+ group. Cognitive impairment showed a negative correlation within the DMN; the lower the functional connectivity in the DMN, the higher the rate of cognitive impairment for the C+ group.

Besides, MVPA in our study discriminated significantly and accurately between groups. A previous work (Kesler et al. 2013) showed similar results concerning the classification performance of MVPA in a group of breast cancer patients. While they significantly distinguished between C+ from both, the C− and the HC groups based on the altered DMN connectivity, the categorization between C- and HC groups was not significant. In contrast, our study achieved a good discrimination power between all groups, with a high sensitivity and specificity. Taken together, our results support the idea that an altered DMN connectivity represents a promising biomarker of the chemotherapy-induced cognitive impairment.

Our study presents some limitations. The cross-sectional design of the study may have limited the possibility to clearly isolate the effect of chemotherapy from more general cancer-related changes. The marked smoking history of both lung cancer groups was a potential confounding variable that may partially explain our DMN disruption results. For this reason, we performed two additional analyses. In the first one, we

focused only on smokers' age-, gender- and education-matched patients (SCLC, $n$ = 6; NSCLC, $n$ = 6 and HC, $n$ = 6), achieving similar results in the DMN connectivity. In the second one, we repeated th e same methodology in an increased group of 21 HC (11 smokers and 10 non-smokers), resulting in non-statistically significant differences between groups.

In conclusion, lung cancer patients prior and following platinum-based chemotherapy treatment exhibit cognitive deficits together with a functional connectivity disruption not only in DMN but also in bilateral temporal and cerebellar regions. While the decrement in DMN connectivity has been related with cancer- and chemotherapy-related cognitive impairment, the increment in bilateral temporal networks found in our study suggests that other brain regions may increase its connectivity to compensate these cognitive deficits.

**Compliance with ethical standards**

**Funding** This work was supported by la Fundació Marató-TV3 [Acquired Spinal Cord and Brain Injuries Program (2012–2015) awarded to ARF] and Hospital of Bellvitge Research Award 2016. Marta Simó is a recipient of a Juan Rodés contract from the Carlos III National Health Institute (Spanish Government)- European Social Fund (ESF).

**Conflicts of interest** All the signing authors have seen and approved the manuscript content and there is no conflict of interest.

**Ethical approval** All procedures performed in studies involving human participants were in accordance with the ethical standards of the institutional and/or national research committee and with the 1964 Helsinki declaration and its later amendments or comparable ethical standards. This article does not contain any studies with animals performed by any of the authors.

**Informed consent** Informed consent was obtained from all individual participants included in the study.

## References

Abou-Elseoud, A., et al. (2010). The effect of model order selection in group PICA. *Human Brain Mapping, 31*(8), 1207–1216. doi:10.1002/hbm.20929.

Ahles, T. A., & Saykin, A. J. (2002). Breast cancer chemotherapy-related cognitive dysfunction. *Clinical Breast Cancer, 3*(Suppl 3), S84–S90.

Ahles, T. A., & Saykin, A. J. (2007). Candidate mechanisms for chemotherapy-induced cognitive changes. *Nature Reviews. Cancer, 7*(3), 192–201. doi:10.1038/nrc2073.

Ahles, T. A., et al. (2002). Neuropsychologic impact of standard-dose systemic chemotherapy in long-term survivors of breast cancer and lymphoma. *Journal of Clinical Oncology, 20*(2), 485–493.

Altman, D. G. (1999). *Practical statistics for medical research*. New York: Chapman & Hall/CRC Press.

Ashburner, J. (2007). A fast diffeomorphic image registration algorithm. *NeuroImage, 38*(1), 95–113. doi:10.1016/j.neuroimage.2007.07.007.

Beckmann, C. F., et al. (2005). Investigations into resting-state connectivity using independent component analysis. *Philosophical Transactions of the Royal Society of London. Series B, Biological Sciences, 360*(1457), 1001–1013. doi:10.1098/rstb.2005.1634.

Bell, A. J., & Sejnowski, T. J. (1995). An information-maximization approach to blind separation and blind deconvolution. *Neural Computation, 7*(6), 1129–1159.

Bruno, J., et al. (2012). Altered resting state functional brain network topology in chemotherapy-treated breast cancer survivors. *Neurobiology of Disease, 48*(3), 329–338. doi:10.1016/j.nbd.2012.07.009.

Buckner, R. L., et al. (2008). The brain's default network: Anatomy, function, and relevance to disease. *Annals of the New York Academy of Sciences, 1124*, 1–38. doi:10.1196/annals.1440.011.

Calhoun, V. D., et al. (2001). A method for making group inferences from functional MRI data using independent component analysis. *Human Brain Mapping, 14*(3), 140–151.

Challis, E., et al. (2015). Gaussian process classification of Alzheimer's disease and mild cognitive impairment from resting-state fMRI. *NeuroImage, 112*, 232–243. doi:10.1016/j.neuroimage.2015.02.037.

Church, J. A., et al. (2009). Control networks in paediatric Tourette syndrome show immature and anomalous patterns of functional connectivity. *Brain, 132*(Pt 1), 225–238. doi:10.1093/brain/awn223.

Cohen, J. (1960). A coefficient of agreement for nominal scales. *Educational and Psychological Measurement, 20*(1), 37–46.

Correa, D. D., et al. (2013). A prospective evaluation of changes in brain structure and cognitive functions in adult stem cell transplant recipients. *Brain Imaging and Behavior*. doi:10.1007/s11682-013-9221-8.

Damoiseaux, J. S. (2012). Resting-state fMRI as a biomarker for Alzheimer's disease? *Alzheimer's Research & Therapy, 4*(2), 8. doi:10.1186/alzrt106.

Damoiseaux, J. S., et al. (2006). Consistent resting-state networks across healthy subjects. *Proceedings of the National Academy of Sciences of the United States of America, 103*(37), 13848–13853. doi:10.1073/pnas.0601417103.

De Luca, M., et al. (2006). fMRI resting state networks define distinct modes of long-distance interactions in the human brain. *NeuroImage, 29*(4), 1359–1367. doi:10.1016/j.neuroimage.2005.08.035.

Dickerson, B. C., et al. (2004). Medial temporal lobe function and structure in mild cognitive impairment. *Annals of Neurology, 56*(1), 27–35. doi:10.1002/ana.20163.

Dietrich, J., et al. (2006). CNS progenitor cells and oligodendrocytes are targets of chemotherapeutic agents in vitro and in vivo. *Journal of Biology, 5*(7), 22. doi:10.1186/jbiol50.

Dumas, J. A., et al. (2013). Chemotherapy altered brain functional connectivity in women with breast cancer: A pilot study. *Brain Imaging and Behavior, 7*(4), 524–532. doi:10.1007/s11682-013-9244-1.

Duzel, E., et al. (2009). Functional imaging of the human dopaminergic midbrain. *Trends in Neurosciences, 32*(6), 321–328. doi:10.1016/j.tins.2009.02.005.

Eichenbaum, H., et al. (2007). The medial temporal lobe and recognition memory. *Annual Review of Neuroscience, 30*, 123–152. doi:10.1146/annurev.neuro.30.051606.094328.

Fawcett, T. (2006). An introduction to ROC analysis. *Pattern Recognition Letters, 27*(8), 861–874.

Franco, A. R., et al. (2009). Interrater and intermethod reliability of default mode network selection. *Human Brain Mapping, 30*(7), 2293–2303. doi:10.1002/hbm.20668.

Gour, N., et al. (2011). Basal functional connectivity within the anterior temporal network is associated with performance on declarative memory tasks. *NeuroImage, 58*(2), 687–697. doi:10.1016/j.neuroimage.2011.05.090.

Gour, N., et al. (2014). Functional connectivity changes differ in early and late-onset Alzheimer's disease. *Hum Brain Mapp, 35*(7), 2978–2994. doi: 10.1002/hbm.22379.

Grosshans, D. R., et al. (2008). Neurocognitive function in patients with small cell lung cancer : Effect of prophylactic cranial irradiation. *Cancer, 112*(3), 589–595. doi:10.1002/cncr.23222.

Hampson, J. P., et al. (2015). Altered resting brain connectivity in persistent cancer related fatigue. *Neuroimage Clinic, 8*, 305–313. doi:10.1016/j.nicl.2015.04.022.

Hillary, F. G., et al. (2015). Hyperconnectivity is a fundamental response to neurological disruption. *Neuropsychology, 29*(1), 59–75. doi:10.1037/neu0000110.

Himberg, J., et al. (2004). Validating the independent components of neuroimaging time series via clustering and visualization. *NeuroImage, 22*(3), 1214–1222. doi:10.1016/j.neuroimage.2004.03.027.

Horky, L. L., et al. (2014). Systemic chemotherapy decreases brain glucose metabolism. *Annals of Clinical Translational Neurology, 1*(10), 788–798. doi:10.1002/acn3.121.

Jim, H. S., et al. (2012). Meta-analysis of cognitive functioning in breast cancer survivors previously treated with standard-dose chemotherapy. *Journal of Clinical Oncology, 30*(29), 3578–3587. doi:10.1200/JCO.2011.39.5640.

Kaasa, S., et al. (1988a). Neuropsychological evaluation of patients with inoperable non-small cell lung cancer treated with combination chemotherapy or radiotherapy. *Acta Oncologica, 27*(3), 241–246.

Kaasa, S., et al. (1988b). Reduced short-term neuropsychological performance in patients with nonsmall-cell lung cancer treated with cisplatin and etoposide. *Antibiotics and Chemotherapy, 41*, 226–231.

Kesler, S. R. (2014). Default mode network as a potential biomarker of chemotherapy-related brain injury. *Neurobiology of Aging, 35*(Suppl 2), S11–S19. doi:10.1016/j.neurobiolaging.2014.03.036.

Kesler, S. R., et al. (2013). Default mode network connectivity distinguishes chemotherapy-treated breast cancer survivors from controls. *Proceedings of the National Academy of Sciences of the United States of America, 110*(28), 11600–11605. doi:10.1073/pnas.1214551110.

Kiviniemi, V., et al. (2009). Functional segmentation of the brain cortex using high model order group PICA. *Human Brain Mapping, 30*(12), 3865–3886. doi:10.1002/hbm.20813.

Komaki, R., et al. (1995). Evaluation of cognitive function in patients with limited small cell lung cancer prior to and shortly following prophylactic cranial irradiation. *International Journal of Radiation Oncology, Biology, Physics, 33*(1), 179–182. doi:10.1016/0360-3016(95)00026-U.

LaViolette, P., Collier, W., Schmainda, K. M., Piacentine, L., Douville, K. L., Chitambar, C. R., Tran, A., Claesges, S. A., Durgerian, S. J., & Bloom, A.S. (2009). International Society for Magnetic Resonance Medicine (ISMRM), Honolulu, HI, USA. In http://cds.ismrm.org/. Functional Connectivity and Arterial Spin Labeling in Chemotherapy Induced Cognitive Impairment ("Chemobrain"). *International Society for Magnetic Resonance Medicine (ISMRM)*.

Lee, M. H., et al. (2013). Resting-state fMRI: A review of methods and clinical applications. *AJNR. American Journal of Neuroradiology, 34*(10), 1866–1872. doi:10.3174/ajnr.A3263.

Lynall, M. E., et al. (2010). Functional connectivity and brain networks in schizophrenia. *The Journal of Neuroscience, 30*(28), 9477–9487. doi:10.1523/JNEUROSCI.0333-10.2010.

Marquand, A., et al. (2010). Quantitative prediction of subjective pain intensity from whole-brain fMRI data using Gaussian processes. *NeuroImage, 49*(3), 2178–2189. doi:10.1016/j.neuroimage.2009.10.072.

Mattis, S. (1988). *Dementia rating scale: Professinal manual*. Odessa: Psychological Assessment Resources.

Mourao-Miranda, J., et al. (2005). Classifying brain states and determining the discriminating activation patterns: Support vector machine on functional MRI data. *NeuroImage, 28*(4), 980–995. doi:10.1016/j.neuroimage.2005.06.070.

O'Reilly, J. X., et al. (2010). Distinct and overlapping functional zones in the cerebellum defined by resting state functional connectivity. *Cerebral Cortex, 20*(4), 953–965. doi:10.1093/cercor/bhp157.

Piccirillo, J. F., et al. (2015). Cognitive impairment after chemotherapy related to atypical network architecture for executive control. *Oncology, 88*(6), 360–368. doi:10.1159/000370117.

Raichle, M. E. (2011). The restless brain. *Brain Connectivity, 1*(1), 3–12. doi:10.1089/brain.2011.0019.

Sanz-Arigita, E. J., et al. (2010). Loss of 'small-world' networks in Alzheimer's disease: Graph analysis of FMRI resting-state functional connectivity. *PloS One, 5*(11), e13788. doi:10.1371/journal.pone.0013788.

Schrouff, J., et al. (2013). PRoNTo: Pattern recognition for neuroimaging toolbox. *Neuroinformatics, 11*(3), 319–337. doi:10.1007/s12021-013-9178-1.

Sheline, Y. I., et al. (2010). Amyloid plaques disrupt resting state default mode network connectivity in cognitively normal elderly. *Biological Psychiatry, 67*(6), 584–587. doi:10.1016/j.biopsych.2009.08.024.

Shilling, V., et al. (2005). The effects of adjuvant chemotherapy on cognition in women with breast cancer–preliminary results of an observational longitudinal study. *Breast, 14*(2), 142–150. doi:10.1016/j.breast.2004.10.004.

Simo, M., et al. (2013). Chemobrain: A systematic review of structural and functional neuroimaging studies. *Neuroscience and Biobehavioral Reviews, 37*(8), 1311–1321. doi:10.1016/j.neubiorev.2013.04.015.

Simo, M., et al. (2015). Cognitive and brain structural changes in a lung cancer population. *Journal of Thoracic Oncology, 10*(1), 38–45. doi:10.1097/JTO.0000000000000345.

Simo, M., et al. (2016a). Longitudinal brain changes associated with prophylactic cranial irradiation in lung cancer. *Journal of Thoracic Oncology, 11*(4), 475–486. doi:10.1016/j.jtho.2015.12.110.

Simo, M., et al. (2016b). Longitudinal brain changes associated with prophylactic cranial irradiation in lung cancer. *Journal of Thoracic Oncology*. doi:10.1016/j.jtho.2015.12.110.

Smith, S. M., et al. (2009). Correspondence of the brain's functional architecture during activation and rest. *Proceedings of the National Academy of Sciences of the United States of America, 106*(31), 13040–13045. doi:10.1073/pnas.0905267106.

Sperling, R. (2007). Functional MRI studies of associative encoding in normal aging, mild cognitive impairment, and Alzheimer's disease. *Annals of the New York Academy of Sciences, 1097*, 146–155. doi:10.1196/annals.1379.009.

Spreng, R. N., & Schacter, D. L. (2012). Default network modulation and large-scale network interactivity in healthy young and old adults. *Cerebral Cortex, 22*(11), 2610–2621. doi:10.1093/cercor/bhr339.

Tate, R. F. (1954). Correlation between a discrete and a continuous variable point-biserial correlation. *The Annals of Mathematical Statistics, 25*(3), 603–607.

Wang, J., et al. (2010). Graph-based network analysis of resting-state functional MRI. *Frontiers in Systems Neuroscience, 4*, 16. doi:10.3389/fnsys.2010.00016.

Wefel, J. S., et al. (2004). The cognitive sequelae of standard-dose adjuvant chemotherapy in women with breast carcinoma: Results of a prospective, randomized, longitudinal trial. *Cancer, 100*(11), 2292–2299. doi:10.1002/cncr.20272.

Welzel, T., et al. (2008). Diffusion tensor imaging screening of radiation-induced changes in the white matter after prophylactic cranial irradiation of patients with small cell lung cancer: First results of a prospective study. *AJNR. American Journal of Neuroradiology, 29*(2), 379–383. doi:10.3174/ajnr.A0797.